A&A 667, A3 (2022)
https://doi.org/10.1051/0004-6361/202243883

Astronomy & Astrophysics

Rayleigh scattering from hydrogen atoms including resonances and high photon energies

René D. Rohrmann and Matías Vera Rueda

Instituto de Ciencias Astronómicas, de la Tierra y del Espacio (CONICET-UNSJ), Av. España 1512 (sur), 5400 San Juan, Argentina
e-mail: rene.rohrmann@conicet.gov.ar

Received 27 April 2022 / Accepted 29 July 2022

ABSTRACT

The nonrelativistic cross section from Rayleigh scattering by hydrogen atoms in the ground state was calculated over a wide range of photon energies (<0.8 keV). Evaluations were performed in terms of the real and imaginary components of the atomic polarizability. The sum over intermediate states that characterizes this second-order radiative process was performed using exact analytic expressions for oscillator strengths of bound and continuum states. Damping terms associated with the finite lifetimes of excited states and their splitting into two fine-structure levels ($p_{1/2}$ and $p_{3/2}$) are taken into account in resonance cross sections. Fitting formulas required for cross-section evaluation are presented for incident photon energy (i) redward of the first resonance (Lyman-$\alpha_{1/2}$), (ii) in the spectral region corresponding to resonances (for an arbitrary number of them), and (iii) above the ionization threshold.

Key words. scattering – atomic processes – opacity

1. Introduction

Rayleigh scattering is potentially relevant to several areas of astronomical spectroscopy including cool stars, star-forming regions, mass-losing stars, exoplanets, the circumgalactic medium, and cosmology. This process significantly affects opacity and emission of the monochromatic radiation field in stellar atmospheres at temperatures of a few thousand Kelvin (Marigo & Aringer 2009). It also provides a diagnostic tool for determining geometrical parameters of double stellar systems containing a giant star (Isliker et al. 1989; González-Riestra et al. 2003; Skopal & Shagatova 2012), and the scale height and composition of exoplanetary atmospheres (Lecavelier Des Etangs et al. 2008; Sing et al. 2015; Dragomir et al. 2015). Rayleigh scattering is especially important in spectroscopy for gaseous nebulae and emission regions of active galactic nuclei (Nussbaumer et al. 1989; Ferland et al. 2017). In addition, scattering of light from isolated hydrogen atoms has an impact on the cosmic microwave background anisotropies. The coupling of photons to neutral hydrogen through Rayleigh scattering during the recombination epoch may have had significant effects on the microwave background fluctuations' spectrum, providing in this way information about the formation of atoms in the early Universe (Scheuer 1965; Gunn & Peterson 1965; Peebles & Yu 1970; Yu et al. 2001; Bach & Lee 2015; Alipour et al. 2015; Beringue et al. 2021).

A coherent scattering cross section including resonances is required for radiation hydrodynamics simulations of late-type stars and accretion disks irradiated by the central star (Hayek et al. 2010; Hirose et al. 2022). It is an important ingredient in self-consistent magneto-hydrodynamical models of solar-type atmospheres which include a chromosphere (Hansteen et al. 2007; Hayek et al. 2010), and in detailed hydrodynamical models of giant stars (Collet et al. 2008; Hayek et al. 2011). Scattering resonances of the Lyman series may affect the temperature structure in the upper atmospheres of cool stars. Specifically, coherent line scattering reduces the temperature by several hundred degrees in the high atmosphere of solar-type stars (Hayek et al. 2010, 2011). This effect could be even the most severe in the low-density giant star atmospheres, resulting in a significantly steeper temperature mean gradient. On the other hand, resonant scattering processes affect the transfer of stellar radiation in protoplanetary disks and have implications on their photochemistry (Neufeld 1991; Bethell & Bergin 2011; Heays et al. 2017).

The present work is motivated by the incompleteness in the compiled set of theoretical Rayleigh cross sections from atomic hydrogen, which is typically limited to wavelengths redward of the Lyman-α resonance (Mittleman & Wolf 1962; Isliker et al. 1989; Lee & Kim 2004; Lee 2005; Fišák et al. 2016; Colgan et al. 2016; Hirose et al. 2022). An exact theoretical description of the Rayleigh scattering by one-electron systems was developed by Gavrila (1967). However, his calculations partially covered only a few resonances and they did not consider damping effects, yielding unphysical singularities. Scattering cross sections from atomic hydrogen have also been calculated by other authors (Nussbaumer et al. 1989; Sadeghpour & Dalgarno 1992; McNamara et al. 2018), but their results have only been presented in a graphical form or over a limited range of photon frequencies and, therefore, they are not useful for computing purposes. In addition, such evaluations neglected fine-structure energy shifts due to relativistic and spin-orbit interaction effects.

The aim of the present work is to expand on the availability of the Rayleigh cross section of neutral hydrogen atoms in the high-photon-energy regime, including an arbitrary number of resonances with excited bound states and taking into account the fine structure and finite lifetimes of such states. Current evaluations correspond to an isolated atom at rest and, therefore, they do not include perturbations arising from collisions with other atoms or Doppler shifts either due to translational motion of the radiating atom.

Rayleigh scattering represents a second-order photon-electron process in the Kramers-Heisenberg dispersion theory

(Kramers & Heisenberg 1925; Waller 1929; Chen & Kotlarchyk 2007). The cross section for photons scattered by $1s$ bound electrons can be computed using the complex atomic polarizability (Bonin & Kresin 1997). Fundamental properties of polarizability and scattering process were first treated by Placzek (1934). Real and imaginary contributions to polarizability are expressed as sums of allowed dipole transitions to intermediate np states, whose well-known oscillator strength values allow for an exact analytic evaluation (Penney 1969). The imaginary part of polarizability has two terms related through the optical theorem to the spectral line absorptions and the photoionization process. Appropriate expressions for the scattering resonance result when level broadening effects are considered (Heddle 1964).

The nonrelativistic dipole approximation adopted here is valid for photon energy much less than $2/\alpha \approx 275$ Rydberg (Ry; Bethe & Salpeter 1957), with $\alpha = 1/137.036$ being the fine-structure constant. In this energy regime, relativistic effects on the dynamical polarizability can be neglected (Johnson & Feiock 1968; Thu et al. 1996; Zapryagaev 2011). For instance, the leading relativistic correction to the static dipole polarizability (nonrelativistic value of 9/2 bohr^3), that is to say in the zero-photon-frequency limit, is $\frac{14}{3}\alpha^2 \approx 1.81 \times 10^{-6}$ (Kaneko 1977). However, corrections to the dynamic dipole polarizability become substantial near resonance peaks due to the corresponding energy shifts and splitting of bound states. Therefore, a semirelativistic model that accounts for the fine-structure effects is sufficient for calculating the cross section of Rayleigh scattering at energies both below and above the ionization threshold.

In Sect. 2, we briefly describe the elastic photon scattering from isolated hydrogen atoms in the ground state through the complex polarizability and the use of transition oscillator strengths. We consider cross section corresponding to unpolarized incident radiation and outgoing radiation averaged over all directions. Section 3 shows the results from numerical calculations done in the infinite level lifetime approximation and neglecting the fine structure. Section 4 is devoted to the analysis of the cross section in the neighborhood of resonances when the natural broadening of excited bound states and the fine structure are taken into account. In Sect. 5, we give functional forms which fit the atomic polarizability. Section 6 presents some evaluations of the Rayleigh cross section. Conclusions are given in Sect. 7.

2. Evaluation of the atomic polarizability

The nonrelativistic cross section of Rayleigh scattering of unpolarized light by a nonoriented hydrogen atom in the ground state, expressed in atomic units (bohr^2), is given by

$$\sigma_{\rm Ra}(\epsilon) = \frac{\pi}{6}\alpha^4\epsilon^4\left|\alpha_{\rm pol}(\epsilon)\right|^2, \tag{1}$$

with ϵ being the photon energy in Rydberg units ($R = 13.60569$ eV), and $\alpha_{\rm pol}(\epsilon)$ being the dynamic polarizability measured in bohr^3. The polarizability is constituted by real and imaginary parts

$$\alpha_{\rm pol} = \alpha_{\rm R} + i\alpha_{\rm I}, \qquad |\alpha_{\rm pol}|^2 = \alpha_{\rm R}^2 + \alpha_{\rm I}^2. \tag{2}$$

They can be expressed in terms of the oscillator strengths of bound states (f_{1n}) and the continuum ($\mathrm{d}f_{1k}/\mathrm{d}\epsilon$),

$$\alpha_{\rm R}^0(\epsilon) = 4\left[\sum_{n=2}^{\infty}\frac{f_{1n}}{\epsilon_{1,n}^2-\epsilon^2} + \mathcal{P}\int_1^{\infty}\frac{\mathrm{d}f_{1k}/\mathrm{d}\epsilon_{1,k}}{\epsilon_{1,k}^2-\epsilon^2}\mathrm{d}\epsilon_{1,k}\right], \tag{3}$$

$$\alpha_{\rm I}^0(\epsilon) = \sum_{n=2}^{\infty}\frac{2\pi}{\epsilon_{1,n}}f_{1n}\delta\left(\epsilon_{1,n}-\epsilon\right) + \frac{2\pi}{\epsilon}\left(\frac{\mathrm{d}f_{1k}}{\mathrm{d}\epsilon}\right), \tag{4}$$

where $\mathcal{P}$ denotes the principal value of the integral, $\delta(x)$ is the Dirac function, and the superscript zero means that bound states are assumed to have infinite lifetimes. In addition, $\epsilon_{1,n}$ and $\epsilon_{1,k}$ are the energies (measured in Rydberg) over the ground state $n' = 1$

$$\epsilon_{n',n} = \frac{1}{n'^2} - \frac{1}{n^2}, \qquad \epsilon_{n',k} = \frac{1}{n'^2} + \frac{1}{k^2}, \tag{5}$$

where n ($= 2, 3, \ldots, \infty$) represents the main quantum number of bound states, and k is a positive real number ($0 < k < \infty$) labeling states in the continuum.

The real part of the polarizability ($\alpha_{\rm R}$) is associated with the refractive index of the medium and can have positive or negative values. The imaginary part of the polarizability ($\alpha_{\rm I}$) is a positive quantity related to the absorption cross section through the optical theorem. In the continuum ($\epsilon > 1$), it corresponds to the photoionization cross section given in bohr^2 by

$$\sigma_{\rm Ph}(\epsilon) = 2\pi\alpha\,\epsilon\,\alpha_{\rm I}. \tag{6}$$

As a reference, the Thomson cross section in the same units is

$$\sigma_{\rm Th} = \frac{8\pi}{3}\alpha^4. \tag{7}$$

Exact expressions for the mean oscillator strength of transitions $1s \to np$ and $1s \to kp$ are well known (Sugiura 1927; Menzel & Pekeris 1935)[1],

$$f_{1n} = \frac{256}{3}\frac{n^5(n-1)^{2(n-2)}}{(n+1)^{2(n+2)}}, \tag{8}$$

$$\frac{\mathrm{d}f_{1k}}{\mathrm{d}\epsilon_{1,k}} = \frac{128}{3}\frac{k^8}{(1+k^2)^4}\frac{\exp\left[-4k\arctan(1/k)\right]}{1-\exp\left[-2\pi k\right]}. \tag{9}$$

The oscillator strength has analytic continuation through the ionization threshold (Fano & Cooper 1968),

$$\lim_{n\to\infty}\left(\frac{n^3}{2}f_{1n}\right) = \lim_{k\to\infty}\left(\frac{\mathrm{d}f_{1k}}{\mathrm{d}\epsilon_{1,k}}\right) = \frac{128}{3\exp(4)} \approx 0.78146725925. \tag{10}$$

Moreover, the asymptotic behavior of the oscillator strength is expressed by the series

$$\frac{n^3}{2}f_{1n} = \frac{128}{3\exp(4)}\left[1 + \frac{8}{3n^2} + \frac{214}{45n^4} + \frac{20192}{2835n^6} + \frac{411683}{42525n^8} + \frac{17369584}{1403325n^{10}} + O\left(n^{-12}\right)\right]. \tag{11}$$

The same expression is valid for $\mathrm{d}f_{1k}/\mathrm{d}\epsilon_{1,k}$ with the substitution $n^2 = -k^2$ ($n = ik$) on the right-hand side of Eq. (11). Direct use of Eqs. (8) and (9) yields numerical errors for high quantum numbers, so we employed Eq. (11) to evaluate f_{1n} and $\mathrm{d}f_{1k}/\mathrm{d}\epsilon_{1,k}$ for $n, k \gg 1$.

The principal value integral in Eq. (3) reduces to a regular integral for $\epsilon < 1$ and the imaginary pole term can be ignored. For $\epsilon > 1$, Cauchy principal value reads as follows:

$$\mathcal{P}\int_1^{\infty}\cdots = \lim_{\delta\to 0}\left(\int_1^{\epsilon-\delta}\cdots + \int_{\epsilon+\delta}^{\infty}\ldots\right). \tag{12}$$

[1] It is worth noting that, for the ground state $n' = 1$, the averaged oscillator strength $f_{n'n}$ is equal to that from the sublevel transition, $f_{n's,np}$.

In practice, the evaluation of this term is split into three subdomains:

$$\mathcal{P}\int_1^{\infty}\cdots = \int_1^{\epsilon-\delta}\cdots + \int_{\epsilon-\delta}^{\epsilon+\delta}\cdots + \int_{\epsilon+\delta}^{\infty}\ldots, \qquad (\delta \ll \epsilon). \quad (13)$$

The second-term integrand on the right-side of Eq. (13) is approximated by its Laurent expansion, where the odd terms about ϵ are removed. Each even term in ϵ can be analytically integrated yielding the following series:

$$\begin{aligned}\int_{\epsilon-\delta}^{\epsilon+\delta}\frac{\mathrm{d}f_{1k}/\mathrm{d}\epsilon_{1,k}}{\epsilon_{1,k}^2-\epsilon^2}\mathrm{d}\epsilon_{1,k} &= \left(-f_\epsilon + 2\epsilon f_\epsilon^{(1)}\right)\frac{\delta}{2\epsilon^2}\\ &+\left(-3f_\epsilon + 6\epsilon f_\epsilon^{(1)} - 6\epsilon^2 f_\epsilon^{(2)} + 4\epsilon^3 f_\epsilon^{(3)}\right)\frac{\delta^3}{72\epsilon^4}\\ &+\left(-15f_\epsilon + 30\epsilon f_\epsilon^{(1)} - 30\epsilon^2 f_\epsilon^{(2)} + 20\epsilon^3 f_\epsilon^{(3)}\right.\\ &\left.-10\epsilon^4 f_\epsilon^{(4)} + 4\epsilon^5 f_\epsilon^{(5)}\right)\frac{\delta^5}{2400\epsilon^6} + O\left(\delta^7\right), \end{aligned} \quad (14)$$

where $f_\epsilon^{(l)}$ is evaluated with (9) as follows:

$$f_\epsilon^{(l)} \equiv \frac{\partial^l(\mathrm{d}f_{1k}/\mathrm{d}\epsilon)}{\partial\epsilon^l}. \quad (15)$$

The first and third integrals on the right-hand side of Eq. (13) were calculated in a standard way using Gaussian quadratures.

3. Results for infinite lifetimes

Expressions (3) and (4) provide high-precision values of $\alpha_{\rm pol}$ far away from resonance cores. This section shows the results of their evaluation. In practice, the sum over bound states in Eq. (3) is truncated to some upper number N:

$$\Sigma_N \equiv \sum_{n=2}^{N}\frac{f_{1n}}{\epsilon_{1,n}^2-\epsilon^2}. \quad (16)$$

Convergence in the evaluation of $\alpha_{\rm R}^0(\epsilon)$ was reached by increasing N and the number of points in the quadratures. Figure 1 shows the sensitivity of Eq. (16) to N. Precision in the sum increases roughly two orders of magnitude for each one-order increase in the number of bound states.

Determining the accuracy by using the use of spectral distribution of oscillator strengths can be done through two simple tests: (i) the Thomas–Reiche–Kuhn f-sum rule

$$\sum_{n=2}^{\infty} f_{1n} + \int_1^{\infty}\frac{\mathrm{d}f_{1k}}{\mathrm{d}\epsilon_{1,k}}\mathrm{d}\epsilon_{1,k} = 1, \quad (17)$$

and (ii) the static polarizability value which is exactly know (Wentzel 1926; Waller 1926; Epstein 1926)[2]:

$$\alpha_{\rm pol}(0) = 4.5\ \mathrm{bohr}^3. \quad (18)$$

As shown in Table 1, both tests can be verified within machine precision. Here, an upper quantum number $N = 10^6$ is adopted.

Figure 2 shows different contributions to the dynamical polarizability as functions of the photon energy. The value

[2] The exact value for the static polarizability of hydrogen atoms can also be obtained by the so-called Dalgarno-Lewis method (Dalgarno & Lewis 1955; Dalgarno & Kingston 1960).

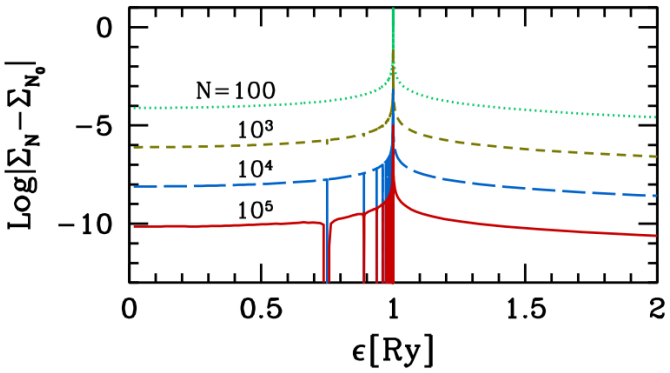

Fig. 1. Accuracy in the evaluation of bound states' contribution to real polarizability, as a function of the photon energy and for different numbers of sum terms in Eq. (16). The reference values Σ_{N_0} correspond to $N_0 = 10^6$. Vertical lines are located on resonances and show a fast convergence effect.

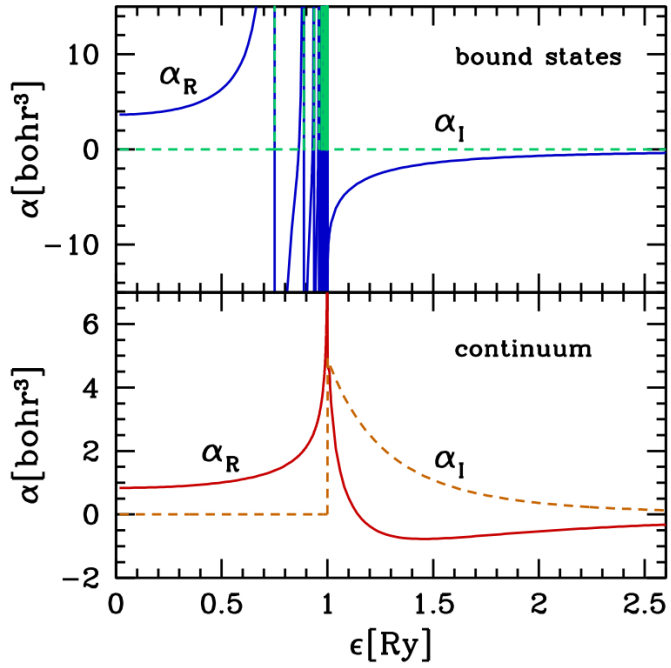

Fig. 2. Variation of the real and imaginary parts of the polarizability due to contributions from bound and continuum states.

Table 1. Contributions to the f-sum rule and static polarizability $\alpha_{\rm pol}(0)$ coming from bound and continuum states.

States	f-sum	$\alpha_{\rm pol}(0)$ (bohr^3)	$\alpha_{\rm pol}(0)$[%]
Discrete	0.5650041506	3.66325789028	81.4057308951
Continuum	0.4349958493	0.83674210969	18.5942691042
All	0.9999999999	4.49999999997	99.9999999993

$\epsilon = 1$ corresponds to the photoelectric threshold for transitions from the $1s$ state. When the natural broadening of the levels is neglected, real and imaginary parts of the polarizability due to bound states become singulars over an infinite sequence of resonances located at energies $\{\epsilon_{1,n}\}$ ($n = 1, 2, \ldots, \infty$), which are distributed at $0.75 \le \epsilon \le 1$ and accumulate on the photoionization edge (upper panel of Fig. 2). In this approach, the

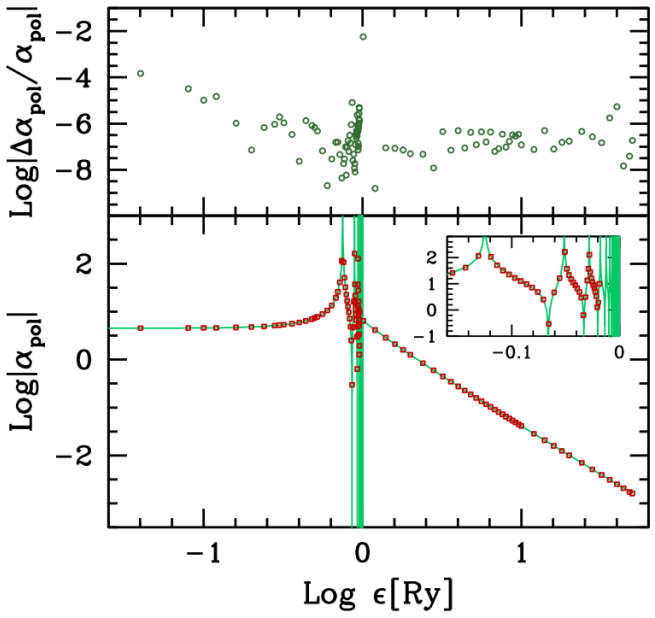

Fig. 3. Dynamic polarizability. *Lower panel*: comparison between the values calculated in the present work (line) and the results of Gavrila (1967, symbols), as a function of the light energy. *Upper panel*: absolute relative errors in a logarithmic scale.

contribution of bound states to $\alpha_{\rm I}^0(\epsilon)$ vanishes for all energies outside of resonances (i.e., $\forall\ \epsilon \neq \epsilon_{1,n}$) according to the set of Dirac functions in Eq. (4).

Contributions of the continuum to polarizability exhibit simple forms (lower panel of Fig. 2). The real part increases monotonically with energy up to $\epsilon = 1$, where it diverges. For energies higher than 1.144210 Ry, $\alpha_{\rm R}$ from the continuum becomes negative and reaches a minimum value of -0.7712916 bohr^3 for $\epsilon \approx 1.4540$. On the other hand, the imaginary part mimics – with a multiplicative factor proportional to ϵ – the behavior of the photoabsorption cross section, according to Eq. (6).

The absolute magnitude of $\alpha_{\rm pol}$ as a function of ϵ is illustrated in logarithmic scales in the lower panel of Fig. 3, where our results (solid line) are compared with those from Gavrila (1967) which are represented by symbols. Relative differences are plotted in the upper panel of Fig. 3. In the limit $\epsilon \to 1^+$, contributions to $\alpha_{\rm R}$ from discrete states and the continuum diverge with opposite signs (see Fig. 2), but they compensate for each other in such a way that total $\alpha_{\rm R}$ remains finite. Therefore, observed divergences of $\alpha_{\rm pol}$ in our evaluations are only produced by resonances, and as a consequence of neglecting the level broadening.

4. Fine-structure and damping effects

When the effects of a fine structure and finite lifetimes of excited bound states are considered, real and imaginary parts of polarization take the forms

$$\alpha_{\rm R}(\epsilon) = 4\left[\sum_{nj}\frac{f_{1,nj}\left(\epsilon_{1,nj}^2-\epsilon^2\right)}{\left(\epsilon_{1,nj}^2-\epsilon^2\right)^2+\epsilon^2\Delta_n^2}+\mathcal{P}\int_1^\infty\frac{{\rm d}f_{1k}/{\rm d}\epsilon_{1k}}{\epsilon_{1,k}^2-\epsilon^2}{\rm d}\epsilon_{1k}\right], \tag{19}$$

$$\alpha_{\rm I}(\epsilon) = \sum_{nj}\frac{4f_{1,nj}\epsilon\Delta_n}{\left(\epsilon_{1,nj}^2-\epsilon^2\right)^2+\epsilon^2\Delta_n^2}+\frac{2\pi}{\epsilon}\left(\frac{{\rm d}f_{1k}}{{\rm d}\epsilon}\right), \tag{20}$$

Table 2. Selection of transition probabilities and natural level breadths.

n	$\epsilon_{1,n}$ (Ry)	Γ (1 s^{-1})	Δ_n (Ry)	χ(fit)(%)	χ(K) (%)
2	0.75	4.69860(8)	2.27307(−8)	+2.04	−39.6
3	0.8888888889	9.98520(7)	4.83061(−9)	+0.17	−31.4
4	0.9375	3.01903(7)	1.46054(−9)	−0.13	−27.1
5	0.96	1.15555(7)	5.59029(−10)	−0.20	−24.4
6	0.9722222222	5.19199(6)	2.51177(−10)	−0.19	−22.5
7	0.9795918367	2.61709(6)	1.26609(−10)	−0.17	−21.0
8	0.984375	1.43796(6)	6.95652(−11)	−0.15	−19.9
9	0.9876543210	8.44833(5)	4.08711(−11)	−0.12	−19.0
10	0.99	5.23645(5)	2.53327(−11)	−0.09	−18.3
11	0.9917355372	3.39069(5)	1.64034(−11)	−0.07	−17.6
12	0.9930555556	2.27687(5)	1.10150(−11)	−0.05	−17.1
13	0.9940828402	1.57668(5)	7.62761(−12)	−0.02	−16.7
14	0.9948979592	1.12094(5)	5.42283(−12)	−0.01	−16.2
15	0.9955555556	8.15308(4)	3.94427(−12)	+0.01	−15.9
16	0.99609375	6.04947(4)	2.92659(−12)	+0.03	−15.5
17	0.9965397924	4.56826(4)	2.21002(−12)	+0.04	−15.2
18	0.9969135802	3.50397(4)	1.69514(−12)	+0.05	−14.9
19	0.9972299169	2.72545(4)	1.31851(−12)	+0.06	−14.7
20	0.9975	2.14670(4)	1.03853(−12)	+0.08	−14.5

Notes. We note that χ(fit) and χ(K) express the relative errors of the Δ_n evaluation using Eq. (24) and the Kramers approximation, respectively. Numbers in brackets indicate powers of 10.

where Δ_n is the natural breadth of the level n and j refers to the two components of each state np ($np_{1/2}$ and $np_{3/2}$). Absorption oscillator strengths of fine-structure transitions are given by the following (Wiese & Fuhr 2009):

$$f_{1,nj=1/2} = \frac{1}{3}f_{1n}, \qquad f_{1,nj=3/2} = \frac{2}{3}f_{1n}. \tag{21}$$

The natural breadth is basically the same for $np_{1/2}$ and $np_{3/2}$ levels, and it can be written in Rydberg units as

$$\Delta_n = \frac{\hbar}{R}\Gamma_n, \qquad \Gamma_n = \sum_{n'=1}^{n-1}A_{nn'}, \tag{22}$$

with $\Gamma_n[{\rm s}^{-1}]$ being the total probability rate of spontaneous decay from n to any lower level, and $A_{nn'}[{\rm s}^{-1}]$ is the Einstein coefficient,

$$A_{nn'} = \frac{\alpha^3 R}{\hbar}\frac{g_{n'}}{g_n}\epsilon_{n',n}^2 f_{n'n} = 8.03250\times10^9[{\rm s}^{-1}]\frac{g_{n'}}{g_n}\epsilon_{n',n}^2 f_{n'n}, \tag{23}$$

with g_n being the statistical weight of the level n. In practice, we calculated Δ_n using accurate $A_{nn'}$ values compiled by Wiese & Fuhr (2009), which expand $n' \leq 19$ and $n \leq 20$ with an uncertainty of less than 0.3%. A precise (within data errors) Δ_n fitting expression for $n \geq 2$ is given by

$$\Delta_n^{\rm fit} = \frac{\alpha^3}{n^5}(-0.187 + 2.915\ln n). \tag{24}$$

Table 2 shows calculated values for natural breadths and probabilities of a spontaneous transition for a selection of levels. Errors of $\Delta_n^{\rm fit}$ are lower than 0.2% for $n \geq 2$. As a reference, evaluations of spontaneous decay probabilities from the well-known Kramers approximation,

$$A_{nn'}^{\rm K} = \frac{32}{3\pi\sqrt{3}}\frac{\alpha^3 R}{\hbar}\frac{1}{n'^3 n^5 \epsilon_{n'n}}, \tag{25}$$

Table 3. Resonances energies (Ry) and wavelengths (Å) of transitions $1s_{1/2}$–$np_{1/2}$ and $1s_{1/2}$–$np_{3/2}$ for $2 \le n \le 20$.

n	$\epsilon(1s_{1/2}, np_{1/2})$	$\epsilon(1s_{1/2}, np_{3/2})$	$\lambda(1s_{1/2}, np_{1/2})$	$\lambda(1s_{1/2}, np_{3/2})$
2	0.7500091526	0.7500124808	1215.67364461	1215.66825001
3	0.8889007225	0.8889017087	1025.72349971	1025.72236178
4	0.9375126368	0.9375130528	972.53767492	972.53724335
5	0.9600129507	0.9600131637	949.74381263	949.74360190
6	0.9722353193	0.9722354426	937.80419396	937.80407506
7	0.9796050110	0.9796050886	930.74897515	930.74890140
8	0.9843882186	0.9843882706	926.22640416	926.22635523
9	0.9876675669	0.9876676034	923.15105870	923.15102457
10	0.9900132636	0.9900132902	920.96378255	920.96375778
11	0.9917488127	0.9917488328	919.35210638	919.35208784
12	0.9930688395	0.9930688549	918.13006685	918.13005260
13	0.9940961302	0.9940961424	917.18127882	917.18126764
14	0.9949112537	0.9949112634	916.42983899	916.42983006
15	0.9955688534	0.9955688613	915.82451267	915.82450541
16	0.9961070504	0.9961070569	915.32969232	915.32968634
17	0.9965530949	0.9965531003	914.92000245	914.91999748
18	0.9969268843	0.9969268889	914.57696078	914.57695660
19	0.9972432223	0.9972432262	914.28684561	914.28684205
20	0.9975133064	0.9975133098	914.03929564	914.03929259

yield Δ_n values with errors between 14% and 40% for $n \le 20$.

Due to relativistic corrections and spin-orbit interaction, each np state splits into two levels with energies (Sobelman 1979)

$$\epsilon_{np_{1/2}} = -\frac{1}{n^2} + \frac{\alpha^2}{n^3}\left(\frac{3}{4n} - 1\right), \quad \epsilon_{np_{3/2}} = -\frac{1}{n^2} + \frac{\alpha^2}{n^3}\left(\frac{3}{4n} - \frac{1}{2}\right), \quad (26)$$

with the zero-energy point in the continuum edge. The ground state ($1s$) remains single ($1s_{1/2}$), but its energy changes from $\epsilon_{1s} = -1$ Ry to

$$\epsilon_{1s_{1/2}} = -1.0000133128 \text{ Ry}. \quad (27)$$

As a consequence, each resonance $1s$–np splits into a doublet with energies

$$\epsilon_{1,nj} = \epsilon_{np_j} - \epsilon_{1s_{1/2}}, \qquad \left(j = \frac{1}{2}, \frac{3}{2}\right), \quad (28)$$

which are slightly higher than that from Eq. (5). They are listed for $n \le 20$ in Table 3 along with the corresponding transition wavelengths (compare them with Kramida 2010).

Polarizability contributions (19) and (20) were evaluated in the way described in Sect. 2. They provide different results than those given by Eqs. (2)–(4) in the neighborhood of each resonance. The first pair of resonances occur around $\epsilon = 0.75$ and correspond to Lyman-$\alpha_{1/2}$ and Lyman-$\alpha_{3/2}$ transitions. Figure 4 shows the module of the polarizability with (solid line) and without (dot-dashed line) a fine structure and damping effects for these resonances. Resonance polarizability given by Eqs. (3) and (4) is redshifted in 1.0816×10^{-5} Ry (line center in $\epsilon_{1,n} = 0.75$ Ry) and its real and imaginary contributions become singulars. On the contrary, imaginary polarizability $\alpha_{\rm I}$ with damping and fine-structure effects (dotted line) presents sharp Lorentzian peaks centered at $\epsilon_{1,2p_{1/2}}$ and $\epsilon_{1,2p_{3/2}}$, with a half width Δ_n. The maximum values of $|\alpha_{\rm pol}|$ coincide with the $\alpha_{\rm I}$ peaks since the real part (dashed line) vanishes there. In fact, the real part of the polarizability tends to be antisymmetric about each resonance center (Fig. 4 shows its absolute value).

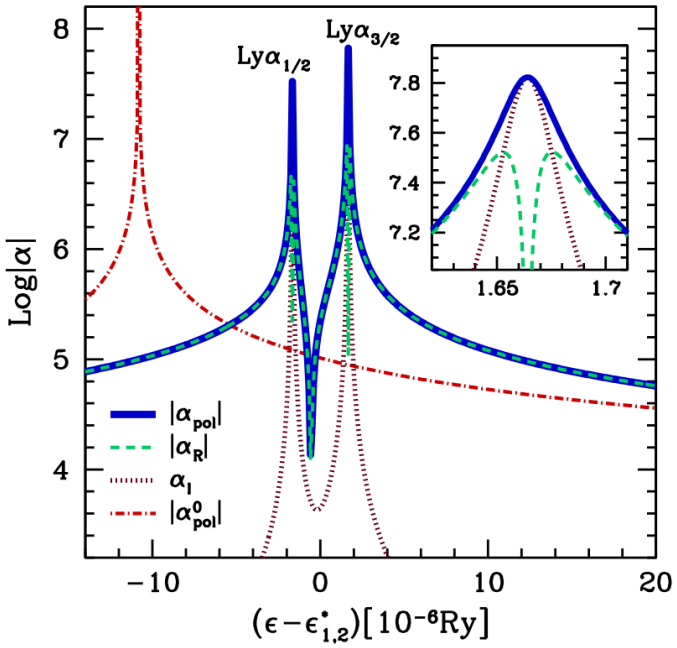

Fig. 4. Polarizability in the Ly$\alpha_{1/2}$ ($1s_{1/2}$–$2p_{1/2}$) and Ly$\alpha_{3/2}$ ($1s_{1/2}$–$2p_{3/2}$) resonances (solid line). We note that $\epsilon^*_{1,2}$ denotes the mean energy of these transitions. Real and imaginary parts of the polarizability are detailed on the plot (dashed and dotted lines, respectively). The inner graph shows details of the Ly$\alpha_{3/2}$ core. Evaluation of Lyman-α resonance without the effects of a fine structure and finite lifetime is represented by a dot-dashed line.

5. Analytic fits

In this section, we provide expressions to evaluate the absolute value of the polarizability. As has been shown, the imaginary part of the polarizability is significant in a very small region around each resonance (Fig. 4) and in the photoionization region due to the continuum contribution (Fig. 2). Therefore, for energies lower than the ionization threshold ($\epsilon < \epsilon_{1s_{1/2}}$) and outside resonance cores, the magnitude of the polarizability ($|\alpha_{\rm pol}|$) is very well approximated by its real part

$$\left|\alpha_{\rm pol}(\epsilon)\right| = |\alpha_{\rm R}(\epsilon)|, \qquad (\epsilon < \epsilon_{1s_{1/2}}, \epsilon \ne \epsilon_{1,nj}). \quad (29)$$

Preresonance region ($\epsilon \lesssim \epsilon_{1,2} = 0.75$ Ry). Redward of Lyman-α, the polarizability is a wellbehaved monotonic function of ϵ and can be approximated with high precision (relative error less than 0.006% at $\epsilon < 0.7496$) by

$$\alpha_{\rm R}(\epsilon) = \frac{1}{1-s}\left(\frac{1.46486}{0.950713 - \epsilon^{2.172}} + \frac{1.66478}{{\epsilon^*_{1,2}}^2 - \epsilon^2}\right), \quad (30)$$

being $\epsilon^*_{1,2} = \frac{1}{2}(\epsilon_{1,2\ j=1/2} + \epsilon_{1,2\ j=3/2})$ and

$$s = \begin{cases} 0.0017 \sin\left(8.2\epsilon^{1.33}\right) - 0.000093 & (\epsilon \le \epsilon_a), \\ -0.00163 \sin\left(16.86\,|\epsilon - \epsilon_a|^{1.2}\right) & (\epsilon_a < \epsilon < 0.73), \\ 0 & (0.73 < \epsilon < 0.745), \\ -10^{-4.9+0.205(0.7501-\epsilon)^{-0.3}} & (0.745 < \epsilon < 0.75), \end{cases} \quad (31)$$

$\epsilon_a = 0.48083$ (for $s \equiv 0$, Eq. (30) has a precision of 0.2%).

Resonance region ($\epsilon_{1,2} \lesssim \epsilon < |\epsilon_{1s_{1/2}}|$). The total polarizability in the resonance region can be reasonably well approximate in the following way. In the neighborhood of a resonance $1s \leftrightarrow np$, the polarizability is well represented keeping only the contributions of $1s_{1/2}$–$np_{1/2}$ and $1s_{1/2}$–$np_{3/2}$ transitions,

$$\alpha_{\rm R}(\epsilon) = \frac{4f_{1,nj=1/2}\left(\epsilon^2_{1,nj=1/2}-\epsilon^2\right)}{\left(\epsilon^2_{1,nj=1/2}-\epsilon^2\right)^2+\epsilon^2\Delta_n^2} + \frac{4f_{1,nj=3/2}\left(\epsilon^2_{1,nj=3/2}-\epsilon^2\right)}{\left(\epsilon^2_{1,nj=3/2}-\epsilon^2\right)^2+\epsilon^2\Delta_n^2}, \tag{32}$$

$$\alpha_{\rm I}(\epsilon) = \frac{4f_{1,nj=1/2}\epsilon\Delta_n}{\left(\epsilon^2_{1,nj=1/2}-\epsilon^2\right)^2+\epsilon^2\Delta_n^2} + \frac{4f_{1,nj=3/2}\epsilon\Delta_n}{\left(\epsilon^2_{1,nj=3/2}-\epsilon^2\right)^2+\epsilon^2\Delta_n^2}. \tag{33}$$

For $\epsilon_{1,nj=3/2} < \epsilon < \epsilon_{1,n+1\ j=1/2}$ ($n = 2, 3, \ldots$), we adopted a fitting formula similar to that one used in Rohrmann (2018)

$$\alpha_{\rm R}(\epsilon) = \frac{\delta_n}{\beta_n}\tan\left[\beta_n\left(\epsilon-\phi_n\right)\right] f(\epsilon), \tag{34}$$

where

$$\beta_n = \begin{cases} \dfrac{\pi}{2(\phi_n-\epsilon_{1,nj=3/2})} & (\epsilon_{1,nj=3/2} < \epsilon < \phi_n), \\ \dfrac{\pi}{2(\epsilon_{1,n+1\ j=1/2}-\phi_n)} & (\phi_n < \epsilon < \epsilon_{1,n+1\ j=1/2}), \end{cases} \tag{35}$$

$$\delta_n = \begin{cases} 315.49655 & (n=2), \\ 15.5183449\times n^{2.9769922}\times(1-A_n)^{-1} & (n>2), \end{cases} \tag{36}$$

$$\phi_n = \epsilon_{1,n+1\ j=1/2} - \left(\epsilon_{1,n+1\ j=1/2}-\epsilon_{1,nj=3/2}\right)B_n, \tag{37}$$

$$f(\epsilon) = (1+C_n\xi)\left\{1-D_n\left[1-(2\xi-1)^2\right]\right\}, \tag{38}$$

$$\xi = \begin{cases} \dfrac{\phi_n-\epsilon}{\phi_n-\epsilon_{1,nj=3/2}} & (\epsilon_{1,nj=3/2} < \epsilon < \phi_n), \\ \dfrac{\epsilon-\phi_n}{\epsilon_{1,n+1\ j=1/2}-\phi_n} & (\phi_n < \epsilon < \epsilon_{1,n+1\ j=1/2}). \end{cases} \tag{39}$$

Quantities A_n, B_n, C_n, and D_n are given as follows:

$$A_n = \begin{cases} 0.1412(2-\log n)^{2.83} & (n \le 100), \\ 0 & (n > 100), \end{cases} \tag{40}$$

$$B_n = \begin{cases} 0.214657809 & (n=2), \\ 0.268 - 10^{-1.2-0.45(\log n)^2-1.61\times10^{-7}(\log n)^{22}} & (n>2). \end{cases} \tag{41}$$

For $\epsilon_{1,nj=3/2} < \epsilon < \phi_n$ and $\phi_n < \epsilon < \epsilon_{1,n+1\ j=1/2}$,

$$C_n = \begin{cases} 0.7346 - 10^{-0.12-1.95\log n+0.035(\log n)^{-2}}, \\ 0.928 - 10^{-0.35-1.65\log n+0.243(\log n)^{-0.43}}, \end{cases} \tag{42}$$

respectively. For $\epsilon_{1,nj=3/2} < \epsilon < \phi_n$,

$$D_n = \begin{cases} 0.245 & (n=2), \\ 0.255 & (3 \le n \le 6), \\ 0.256 - 10^{-1.15-0.22(\log n-0.6)^{-1.12}} & (n>6), \end{cases} \tag{43}$$

and for $\phi_n < \epsilon < \epsilon_{1,n+1\ j=1/2}$,

$$D_n = 0.053 - 10^{-0.44-1.965(\log n)^{0.6}}. \tag{44}$$

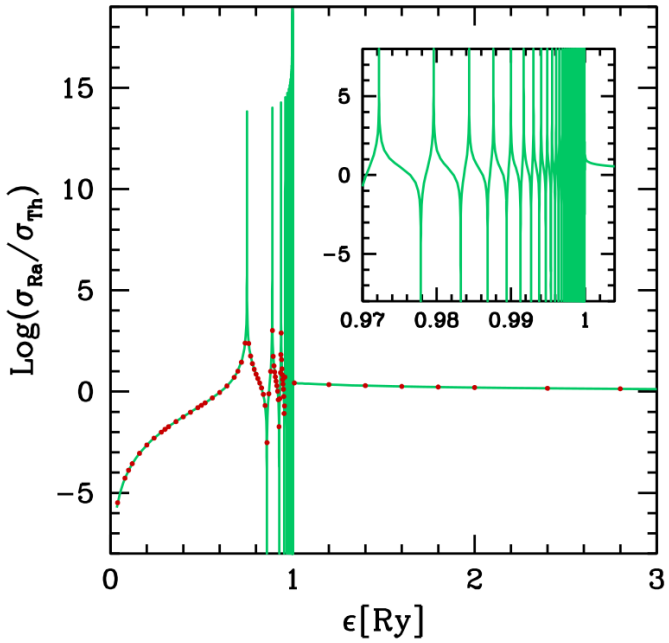

Fig. 5. Rayleigh cross section in units of the Thompson cross section as a function of the photon energy. The solid line represents evaluations with Eq. (1) combined with Eqs. (19) and (20). Symbols represent the results from Gavrila (1967).

The quantity ϕ_n represents the energy between two resonances where the real polarizability vanishes. Eq. (41) gives B_n (the position of ϕ_n relative to $\epsilon_{1,n\ j=3/2}$ and $\epsilon_{1,n+1\ j=1/2}$, see Eq. (37)) with an error <0.5% $\forall$ n and below 0.02% for $n \gtrsim 30$ (precision increasing with n). Just outside of resonance cores, where imaginary polarizability is not significant, Eq. (34) describes the total polarizability redward of $\epsilon_{1,n\ j=1/2}$ with a precision better than 0.9% $\forall n$, 0.5% for $n > 9$ and 0.2% for $n > 16$. Blueward of $\epsilon_{1,n\ j=3/2}$, the relative error is 1.8% for $n = 2$, 1.6% for $n = 3$, <0.85% for $n \ge 4$, and <0.2% for $n \ge 20$.

Postresonance region ($\epsilon > |\epsilon_{1s_{1/2}}| = 1.0000133128$ *Ry*). For large values of ϵ, the nonrelativistic Rayleigh cross section converges to the Thomson scattering cross section. This means

$$\left|\alpha_{\rm pol}(\epsilon)\right| \to 4\epsilon^{-2}, \qquad (\epsilon \gg 1). \tag{45}$$

A precision better than 0.4% (relative error) for the polarizability above the ionization threshold was obtained with

$$\left|\alpha_{\rm pol}(\epsilon)\right| = \frac{4}{\epsilon^2}\left[1+\frac{0.6262}{1+2.8179\epsilon^{0.6776}\left(1+0.0216672\epsilon^{1.4745}\right)\log\epsilon}\right]. \tag{46}$$

6. Scattering cross section

The Rayleigh scattering cross section was obtained simply by multiplying $|\alpha_{\rm pol}|^2$ by the factors appearing in Eq. (1). The Rayleigh cross section for hydrogen atoms obtained in this work is displayed in Fig. 5. Current calculations (solid line) include about one hundred resonances which have finite amplitudes. These results are in very good agreement with those derived from Gavrila (1967) in the limited number of energies presented there (symbols), which do not include resonance cores. For high enough energies, in the regime where the dipole approximation

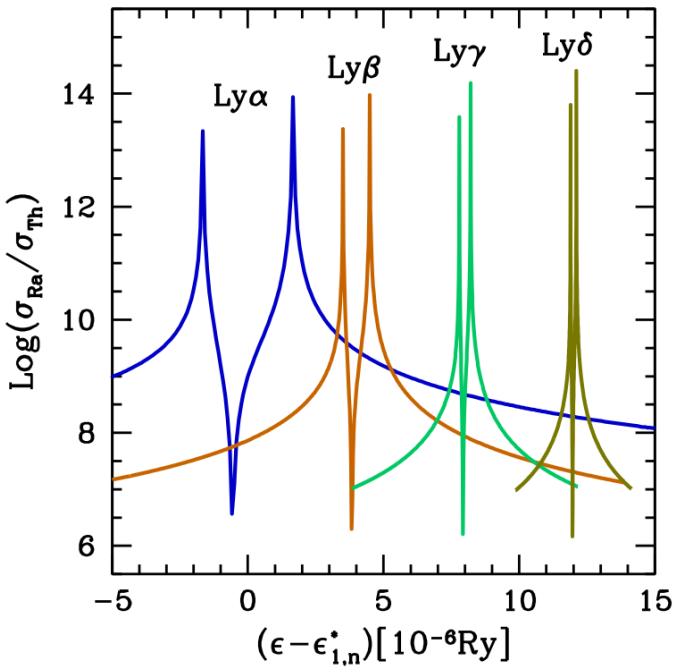

Fig. 6. Rayleigh cross section for the first four double resonances, from Lyman-α to Lyman-δ, computed with a fine structure and damping effects. Profiles are horizontally offset from each other in steps of 4×10^{-6} Ry.

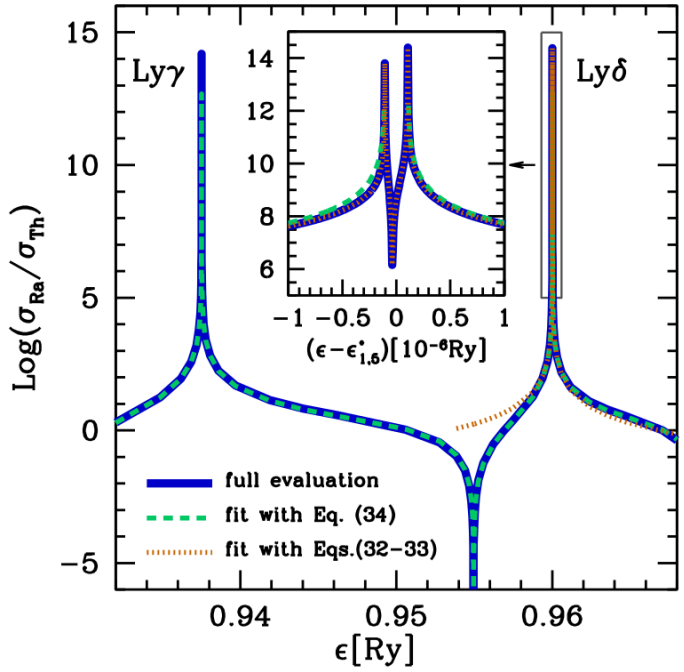

Fig. 7. Rayleigh cross section for photon energies including the resonances Lyman-γ and Lyman-δ. Solid lines represent full solutions based on Eqs. (19) and (20). Dashed and dotted lines correspond to fitting evaluations with Eqs. (34) and (32)–(33), respectively. The inner graph shows the core of Lyman-δ.

still holds, the cross section slowly approaches the expected Thomson formula.

It should be noted that the energy interval between successive n states, the separation between fine-structure components, and the natural breadth of the levels scale with α and n in the form

$$E_{n+1} - E_n \approx \frac{2}{n^3}, \quad \Delta E_{\text{fine structure}} = \frac{\alpha^2}{2n^3}, \quad \Delta_n \approx \frac{3\alpha^3 \ln(n)}{n^5}. \tag{47}$$

The first of these relations describes the distribution of resonances $1s$–np and their accumulation on the photoionization edge (Fig. 5). The other two relations characterize the shape of each of these (double) resonances, as shown in Fig. 6. The natural width of the resonances becomes small enough and decreases very quickly as the main quantum number n of the excited state increases faster than the energy separation between fine structure components. Consequently, the profiles of successive resonances are progressively narrower and the magnitude of $|\alpha_{\text{pol}}|$ in their peaks increases with n. Relative intensities of $1s_{1/2}$–$np_{1/2}$ and $1s_{1/2}$–$np_{3/2}$ resonances are proportional to the ratio 1:2 of their oscillator strengths, which are in turn proportional to the statistical weights of sublevels $np_{1/2}$ and $np_{3/2}$, see Eq. (21).

As an illustration, Fig. 7 compares the use of polarizability fits in the evaluation of the Rayleigh cross section within the resonance region. Fits based on Eq. (34) give satisfactory results where the cross section changes many orders of magnitude over energy intervals between successive resonances. On the other hand, Eqs. (32) and (33) match – with high accuracy – the resonance cores including fine-structure details. In astrophysical conditions where the fine-structure splitting can be considered negligible, Eqs. (32) and (33) can be substituted by

$$\left|\alpha_{\text{pol}}(\epsilon)\right| = 4 f_{1n} \left[({\epsilon^*_{1,n}}^2 - \epsilon^2)^2 + (\epsilon \Delta_n)^2 \right]^{-1/2}, \tag{48}$$

where $\epsilon^*_{1,n}$ is the mean energy of the transition $1s - np$.

Current calculations were performed for an isolated atom. It is worth noting that in a realistic plasma, where broadening mechanisms are present due to particle perturbations (collisional broadening) and thermal motions (Doppler broadening), resonance profiles are expected to be significantly broader than those of an isolated radiating atom (Omont et al. 1972, 1973; Nienhuis & Schuller 1977; Burnett 1985). Moreover, interactions with surrounding ions and electrons particularly affect highly excited np states and introduce modifications in the cross section close to the photoionization threshold (Griem 2005).

7. Conclusions

We have performed an accurate numerical evaluation of the Rayleigh scattering cross section for hydrogen atoms in the ground state, including resonances and incident photon energies above the ionization threshold. Current evaluations were carried out using the nonrelativistic dipole approximation in the second-order standard quantum perturbative approach. Due to symmetries of the hydrogen ground state, the calculation can be focused on the atomic polarizability which is expressed in terms of the oscillator strengths' distribution. The method is valid for incident photon energies above and below the ionization threshold. It involves a summation over all intermediate electron states which is split into a sum over bound states and a Cauchy principal value integral over the continuum with an imaginary pole term. Convergence in evaluations is achieved by increasing the number of intermediate bound states and quadrature points.

Our results for Rayleigh scattering are in good agreement with available theoretical data and they expand upon them with a detailed representation of the resonances' region and the incorporation of a fine structure of the bound levels and damping

effects due to finite lifetimes of the excited bound states. We provide fitting formulas to obtain the Rayleigh scattering cross sections in the full nonrelativistic domain, as is required for opacity calculations and their use in astrophysical computer codes.

Acknowledgements. We wish to thank Shigenobu Hirose, who put our attention on current issue. We also thank the anonymous referee for the constructive remarks. This work was supported by MINCYT (Argentina) through Grant No. PICT 2016-1128.

References

Alipour, E., Sigurdson, K., & Hirata, C. M. 2015, Phys. Rev. D, 91, 083520
Bach, K., & Lee, H.-W. 2015, MNRAS, 446, 264
Beringue, B., Meerburg, P. D., Meyers, J., & Battaglia, N. 2021, J. Cosmology Astropart. Phys., 2021, 060
Bethe, H. A., & Salpeter, E. E. 1957, Quantum Mechanics of One- and Two-Electron Atoms, 298
Bethell, T. J., & Bergin, E. A. 2011, ApJ, 739, 78
Bonin, K.D. & Kresin, V.V. 1997, Electric-dipole polarizabilities of atoms, molecules, and clusters, 20
Burnett, K. 1985, Phys. Rep., 118, 339
Chen, S.-H., & Kotlarchyk, M. 2007, Interactions of Photons and Neutrons with Matter (World Scientific), 425
Colgan, J., Kilcrease, D. P., Magee, N. H., et al. 2016, ApJ, 817, 116
Collet, R., Asplund, M., & Trampedach, R. 2008, Mem. Soc. Astron. Italiana, 79, 649
Dalgarno, A., & Kingston, A. E. 1960, Proc. Roy. Soc. Lond. A, 259, 424
Dalgarno, A., & Lewis, J. T. 1955, Proc. Roy. Soc. Lond. A, 233, 70
Dragomir, D., Benneke, B., Pearson, K. A., et al. 2015, ApJ, 814, 102
Epstein, P. S. 1926, Phys. Rev., 28, 695
Fano, U., & Cooper, J. W. 1968, Rev. Mod. Phys., 40, 441
Ferland, G. J., Chatzikos, M., Guzmán, F., et al. 2017, Rev. Mexicana Astron. Astrofis., 53, 385
Fišák, J., Krtička, J., Munzar, D., & Kubát, J. 2016, A&A, 590, A95
Gavrila, M. 1967, Phys. Rev., 163, 147
González-Riestra, R., Rossi, C., & Viotti, R. F. 2003, A&A, 399, 681
Griem, H. R. 2005, Principles of Plasma Spectroscopy, 147
Gunn, J. E., & Peterson, B. A. 1965, ApJ, 142, 1633
Hansteen, V. H., Carlsson, M., & Gudiksen, B. 2007, in Astronomical Society of the Pacific Conference Series, 368, The Physics of Chromospheric Plasmas, eds. P. Heinzel, I. Dorotovič, & R. J. Rutten, 107
Hayek, W., Asplund, M., Carlsson, M., et al. 2010, A&A, 517, A49
Hayek, W., Asplund, M., Collet, R., & Nordlund, Å. 2011, A&A, 529, A158
Heays, A. N., Bosman, A. D., & van Dishoeck, E. F. 2017, A&A, 602, A105
Heddle, D. W 1964, Journal of the Optical Society of America, 54, 264
Hirose, S., Hauschildt, P., Minoshima, T., Tomida, K., & Sano, T. 2022, A&A, 659, A87
Isliker, H., Nussbaumer, H., & Vogel, M. 1989, A&A, 219, 271
Johnson, W. R., & Feiock, F. D. 1968, Phys. Rev., 168, 22
Kaneko, S. 1977, J. Phys. B At. Mol. Phys., 10, 3347
Kramers, H. A., & Heisenberg, W. 1925, Z. Physik, 31, 681
Kramida, A. E. 2010, At. Data Nucl. Data Tables, 96, 586
Lecavelier Des Etangs, A., Pont, F., Vidal-Madjar, A., & Sing, D. 2008, A&A, 481, L83
Lee, H.-W. 2005, MNRAS, 358, 1472
Lee, H.-W., & Kim, H. I. 2004, MNRAS, 347, 802
Marigo, P., & Aringer, B. 2009, A&A, 508, 1539
McNamara, K., Fursa, D. V., & Bray, I. 2018, Phys. Rev. A, 98, 043435
Menzel, D. H., & Pekeris, C. L. 1935, MNRAS, 96, 77
Mittleman, M. H., & Wolf, F. A. 1962, Phys. Rev., 128, 2686
Neufeld, D. A. 1991, ApJ, 370, L85
Nienhuis, G., & Schuller, F. 1977, Physica B+C, 92, 397
Nussbaumer, H., Schmid, H. M., & Vogel, M. 1989, A&A, 211, L27
Omont, A., Smith, E. W., & Cooper, J. 1972, ApJ, 175, 185
Omont, A., Smith, E. W., & Cooper, J. 1973, ApJ, 182, 283
Peebles, P. J. E., & Yu, J. T. 1970, ApJ, 162, 815
Penney, C. M. 1969, J. Opt. Soc. Am., 59, 34
Placzek, G. 1934, Handbuch der Radiologie, VI (Akademische Verlagsgesellschaft, Leipzig), 2, 209
Rohrmann, R. D. 2018, MNRAS, 473, 457
Sadeghpour, H. R., & Dalgarno, A. 1992, J. Phys. B At. Mol. Phys., 25, 4801
Scheuer, P. A. G. 1965, Nature, 207, 963
Sing, D. K., Wakeford, H. R., Showman, A. P., et al. 2015, MNRAS, 446, 2428
Skopal, A., & Shagatova, N. 2012, A&A, 547, A45
Sobelman, I. I. 1979, Atomic spectra and radiative transitions (Berlin: Springer)
Sugiura, Y. 1927, J. Phys. Radium, 8, 113
Thu, L., Hoang, L., Komarov, L. I., & Romanova, T. S. 1996, J. Phys. B At. Mol. Phys., 29, 2897
Waller, I. 1926, Z. Physik, 38, 635
Waller, I. 1929, Z. Physik, 58, 75
Wentzel, G. 1926, Z. Physik, 38, 518
Wiese, W. L., & Fuhr, J. R. 2009, J. Phys. Chem. Ref. Data, 38, 1129
Yu, Q., Spergel, D. N., & Ostriker, J. P. 2001, ApJ, 558, 23
Zapryagaev, S. 2011, Physica Scripta T, 144, 014053